Additive Manufacturing for Self-Healing Soft Robots

Roels, Ellen; Terryn, Seppe; Brancart, Joost; Verhelle, Robrecht René; Van Assche, Guy; Vanderborght, Bram

Published in:
Soft Robotics

DOI:
10.1089/soro.2019.0081

Publication date:
2020

Document Version:
Final published version

SOFT ROBOTICS
Volume 7, Number 6, 2020

DOI: 10.1089/soro.2019.0081

SoRo
Soft Robotics

ORIGINAL ARTICLE

Additive Manufacturing for Self-Healing Soft Robots

Ellen Roels,[1–3] Seppe Terryn,[1–3] Joost Brancart,[3] Robrecht Verhelle,[3] Guy Van Assche,[3] and Bram Vanderborght[1,2]

Abstract

The field of self-healing soft robots was initiated a few years ago. A healing ability can be integrated in soft robots by manufacturing their soft membranes out of synthetic self-healing polymers, more specifically elastomeric Diels–Alder (DA) networks. As such they can recover completely from macroscopic damage, including scratches, cuts, and ruptures. Before this research, these robots were manufactured using a technique named ''shaping-through-folding-and-self-healing.'' This technique requires extensive manual labor, is relatively slow, and does not allow for complex shapes. In this article, an additive manufacturing methodology, fused filament fabrication, is developed for the thermoreversible DA polymers, and the approach is validated on a soft robotic gripper. The reversibility of their network permits manufacturing these flexible self-healing polymers through reactive printing into the complex shapes required in soft robotics. The degree of freedom in the design of soft robotics that this new manufacturing technique offers is illustrated through the construction of adaptive DHAS gripper fingers, based on the design by FESTO. Being constructed out of self-healing soft flexible polymer, the fingers can recover entirely from large cuts, tears, and punctures. This is highlighted through various damage–heal cycles.

Keywords: additive manufacturing, fused filament fabrication, soft robot materials and manufacturing, self-healing materials, Diels–Alder polymers

Objective

Using nature as a source of inspiration, soft robotics is a fast advancing research field.[1] Soft actuators are manufactured from a wide range of flexible materials, such as polymers, for example, elastomers[2,3] or fabrics,[4] and composites.[5] Their inherent compliance allows for safe interaction with their environment,[6] which potentially can include humans.[7] The soft actuators these robotic systems consist of are often based on inflatable or hydraulic voids,[8] or actuated by tendons connected to an electric motor.[2,9]

Although their compliance protects them from shocks,[6] the flexibility and softness of these robotic parts have a major drawback: they are more prone to tearing, piercing, and other forms of damage, besides the usual wear and fatigue. This occurs when handling sharp objects or while operating in a dynamic unpredictable environment containing sharp or pointy items. Amend *et al.* state that their commercial jamming gripper (Versaball) has its lifetime reduced from 50,000 to 5000 grips in these situations.[10] In pneumatically actuated parts, leaks can result from applying extensive overpressure on the inner chamber of the soft pneumatic actuator. If the leak is limited in size, this damage does not lead to the full failure of the actuator; however, it results in a loss in efficiency, a loss in maximum force output, and affects the actuator dynamics or performances.

To prevent damage in soft robots, the current trend is to overdimension their components, which results in heavier and larger designs, which are more expensive and less energy efficient.[11]

An alternative solution for the susceptibility of these soft devices is to construct them from synthetic self-healing polymers. These reversible polymer networks employ healing mechanisms based on different chemistries, such as physicochemical bonds, such as hydrogen bonds[12,13] or reversible covalent bonds, such as those formed in the Diels–Alder (DA) reaction.[14,15] In prior study, the authors developed the first demonstrators of self-healing soft robotics, including soft grippers, soft hands, and artificial muscles.[16,17] These actuators have shown a recovery of up to 98%[16] after severe damage, leaving no weak spots.

[1]Robotics and Multibody Mechanics (R&MM), Vrije Universiteit Brussel, Brussels, Belgium.
[2]Flanders Make, Brussels, Belgium.
[3]Physical Chemistry and Polymer Science (FYSC), Vrije Universiteit Brussel, Brussels, Belgium.

The self-healing polymer networks used are cross-linked by thermoreversible DA bonds.[18] The healing of these networks is intrinsic and is accelerated by mild heating (<90°C) to trigger and continue the healing process. Recent research has proved that through tuning of the material properties during synthesis, DA cross-linked networks can be developed that allow healing at room temperature.[19] In addition, multiple synthesis design parameters allow tuning the mechanical and processing properties of DA networks.[16] Brittle glassy self-healing thermoset networks can be synthesized as well as hyperflexible elastomers with high fracture strains. Although having dissimilar mechanical properties, these different materials can chemically bind at the interface through a heat–cool cycle, resulting in a very strong connection.[20]

The self-healing soft actuators were developed through a new technique, referred to as ''shaping-through-folding-and-self-healing.''[21] Finding inspiration in origami, this method exploits the healing ability in the manufacturing phase. Polygon structures are formed by consecutively folding and merging sheets through mild heat cycles. This technique permits combining multiple self-healing DA materials, with contrasting mechanical properties, in a single component.[20] However, when the complexity of the component is increased, extensive manual labor is required and the process becomes time consuming.

In general, soft robots are manufactured by lithography[22] and molding, including compression molding,[23] and casting.[20,24] Only recently, flexible materials for additive manufacturing (e.g., NinjaFlex, FilaFlex, and Cheetah) are being commercialized. These allow using selective laser sintering,[25] stereolithography,[26] direct ink writing,[27,28] or fused filament fabrication (FFF)[29,30] (also known under the trademarked name ''fused deposition modeling'') for the construction of soft robotic components.

Recently, first reports of the additive manufacturing of reversible polymer networks have appeared in the literature.[31] In 2017, Yang *et al.* published a feasibility study on the printing of a reversible DA polymer network using a syringe extrusion method, starting from a hot polymer liquid.[32] In 2019, Yu *et al.* reported a stereolithography method to print a photocurable acrylate.[33] Although the latter technique does not utilize the reversibility or self-healing property of the material, the final printed material does possess self-healing properties by means of disulfide bonds.

In this article, a novel additive manufacturing procedure based on filament extrusion is developed for a self-healing elastomer, exploiting the thermoreversibility of the network formation. The article continues with the Materials and Methods section, in which a detailed description on the monomer materials used to synthesize the DA networks is given, followed by a brief introduction in the reaction kinetics of the DA reaction and on the analysis methods used.

The Material Properties section gives in detail about the extrusion and printing conditions, combined with a thorough characterization of the material.

The Results section describes how this self-healing elastomer is extruded into filament and printed using FFF. In A 3D-Printed Self-Healing Soft Actuator section, these new developments are used to manufacture a soft gripper designed by FESTO, for which both the picking and healing abilities of this gripper are validated.

Materials and Methods

Materials

The self-healing materials used in this study are reversible polymer networks, the concept of which is illustrated in Figure 1. The network is formed using two building blocks: furan-functionalized Jeffamines (FGE-JT5000) are reversibly cross-linked by 1,1′-(methylenedi-4,1-phenylene)bismaleimide (DPBM), respectively, colored as orange and blue in Figure 1. The DA reaction between a furan and a maleimide group is a reversible cycloaddition reaction, combining the forward bond-forming reaction and the reverse bond-breaking retro DA reaction, as shown in Figure 2a.

To synthesize the material, furfuryl glycidyl ether (FGE) (Fig. 2c) reacts first irreversibly with a Jeffamine (Fig. 2b). This furan-functionalized Jeffamine is afterward mixed with DPBM in a stoichiometric ratio between maleimide and furan, and subsequently dissolved in chloroform (20 wt%). Hydroquinone (Fig. 2e) is added as a radical inhibitor to prevent irreversible side reactions (Michael addition, maleimide homopolimerization).[16] The detailed synthesis steps are described by Scheltjens *et al.*[18] Although the separate monomers used for the synthesis of these materials are known to cause issues such as skin and eye irritation, almost all functional groups that account for this possible toxicity are bonded in the postgel state. Therefore, there are no small molecules to which a user is exposed during normal usage that can lead to harmful effects.

Traditionally, polymer network materials (e.g., epoxy–amine systems or vulcanized rubbers) are irreversibly cross-linked. In contrast to linear or branched thermoplastics, these materials cannot be reprocessed as the permanent network prevents flow at higher temperatures. The DA polymers studied in this work are reversibly cross-linked, meaning they have a reversible gel transition that happens at the gel temperature (T_{gel}) (Fig. 1). When kept at temperatures $<T_{gel}$, the material forms a single network molecule and the molecular weight shifts toward infinity (gelation), resulting in an elastic behavior.

Above this temperature, enough bonds break, so that there is no longer a network (degelation) that results in a viscous flow behavior. As kinetics are faster at higher temperatures, gelation happens the fastest at temperatures near (but still

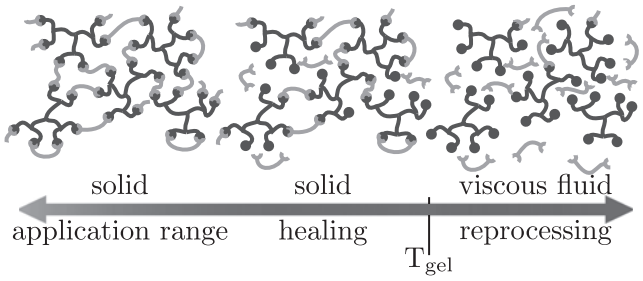

FIG. 1. The self-healing polymer is reversibly cross-linked by DA bonds. At low temperatures (room temperature), the material polymer is in a network structure that provides structural stability, and can be used for the intended application. When increasing the temperature, a fraction of the DA cross-links break, increasing the molecular mobility, which allows healing macroscopic damages. Above the gel temperature (T_{gel}), there is viscous flow and the polymer can be reprocessed. Reproduced from Roels *et al.*[20] DA, Diels–Alder.

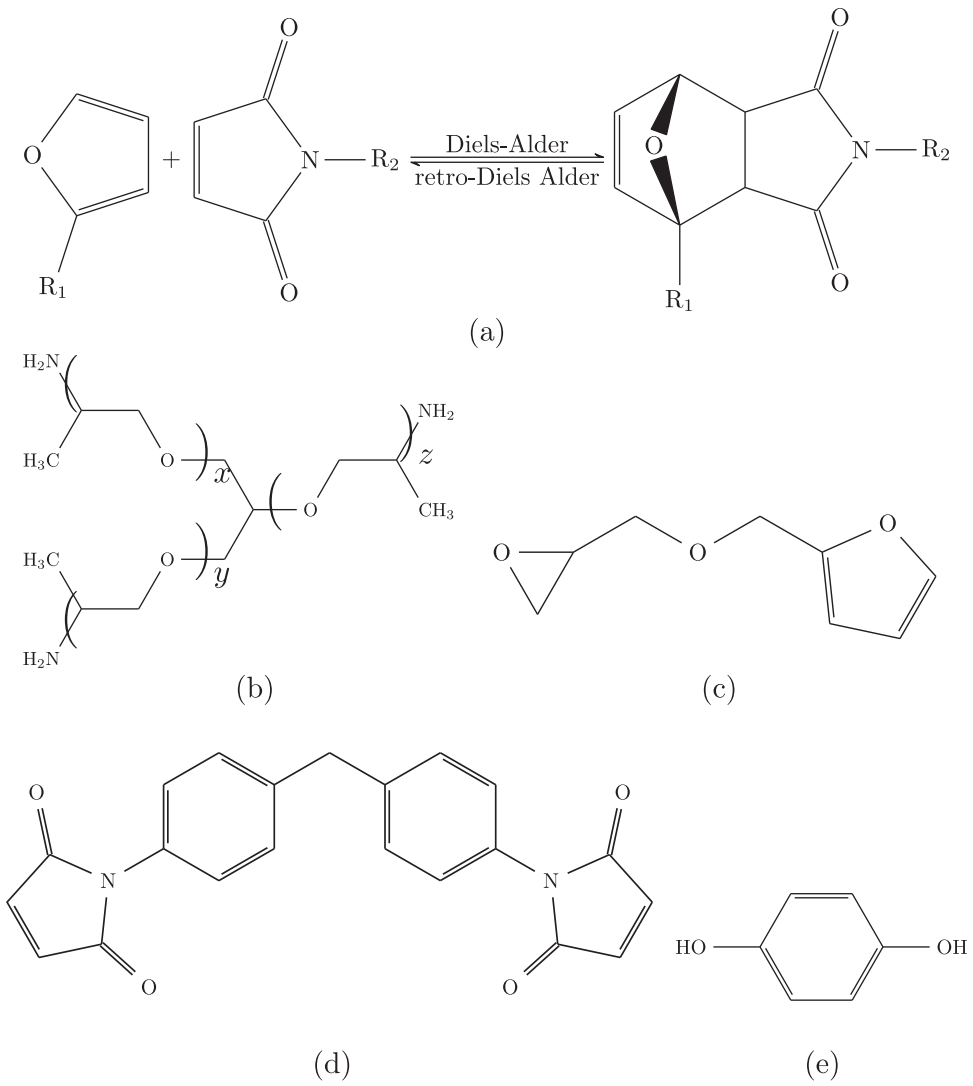

FIG. 2. **(a)** A DA reaction is an equilibrium reaction between a diene (furan) and a dienophile (maleimide) and forms a cyclohexene (DA adduct). **(b–e)** Monomers of DPBM-FGE-JT5000 (in short DPBM-FT5000). **(b)** Tertiary Jeffamine (JT5000): $x + y + z \approx 85$, $M = 5649$ g/mol, by Aurora Chemicals. **(c)** FGE, 154 g/mol, 96% purity, by Sagechem. **(d)** DPBM, 265 g/mol, 95% purity, by Sigma Aldrich. **(e)** Hydroquinone by Chimica. DPBM, 1,1′-(methylenedi1,4-phenylene) bismaleimide; FGE, furfuryl glycidyl ether.

below) T_{gel}.[15] Degelation happens faster at higher temperatures, but care has to be taken, as irreversible side reactions can occur >120°C.[21]

One of the interesting abilities of this polymer is the possibility to vary its mechanical and processing properties. By varying the type of Jeffamine used to create the furan-functionalized compounds, the mechanical properties and thermal behavior of the formed network can be tuned for the intended application and optimized for the manufacturing processes. The length of Jeffamine controls the spacer length between the thermoreversible cross-links, and consequently the DA cross-link density. When this length is short, the overall cross-link density, thus the concentration of the thermoreversible covalent bonds is higher and the material will be stiffer and more brittle.[16] A long spacer length results in a lower cross-link density and a more flexible material, which is desired for the intended soft robotics application.

For FFF, the material needs to have sufficiently fast solidification kinetics, thus a high processing temperature is preferred. However, it should not be so high that the material degrades or forms irreversible bonds. There are several ways the gelation (solidification) of the DA materials can be improved. In this study, a six-functional furan compound (FT5000) is used, which has a lower gel conversion x_{gel} than the four-functional compound used in previous studies[16,17] and thus has a higher T_{gel} and solidifies faster. Keeping all constraints in mind, the self-healing DA material DPBM-FT5000 in stoichiometric ratio ($R = \frac{n_{maleimide}}{n_{furan}} = 1$) was selected for this application.

Reaction kinetics

In a previous study, the authors reported the effect of stereochemistry of the DA reaction.[15] A detailed discussion about the stereochemistry of the cycloaddition is out of scope for this article; however, for the kinetic simulations of the material behavior, the formation of two stereoisomers is taken into account as they have different rate constants k.

$$A_{endo} \underset{k_{endo}}{\overset{k_{r,\,endo}}{\rightleftharpoons}} F + M \underset{k_{r,\,exo}}{\overset{k_{exo}}{\rightleftharpoons}} A_{exo}. \quad (1)$$

Each of these rate constants is calculated using the Arrhenius equation

$$k = Ae^{\frac{-E_A}{RT}}, \tag{2}$$

where
k is rate constant,
A is pre-exponential factor,
E_A is activation energy,
R is universal gas constant, and
T is absolute temperature,
which also shows that the equilibrium is temperature dependent. The reaction rates are increased at higher temperatures. For every reaction, the activation energy and the pre-exponential factor are determined experimentally.

A set of ordinary differential equations describes the variation of the concentration of all components in the DA equilibrium reaction (i = endo, exo).

$$\frac{d[M]}{dt} = \sum_{i=\text{endo, exo}} (k_{r,i}[A_i] - k_i[M][F]) \tag{3}$$

$$= \frac{d[F]}{dt} \tag{4}$$

$$\frac{d[A_i]}{dt} = k_i[M][F] - k_{r,i}[A_i]. \tag{5}$$

The total conversion x_{tot}, calculated by integration of

$$\frac{x_{tot}}{dt} = \frac{x_{endo}}{dt} + \frac{x_{exo}}{dt} \tag{6}$$

$$= \frac{1}{[M_0]}\left(\frac{d[A_{endo}]}{dt} + \frac{d[A_{exo}]}{dt}\right), \tag{7}$$

is the ratio of the amount of DA bonds formed in the polymer network over the maximum possible amount of bonds that could be formed, equal to the initial maleimide concentration $[M_0]$. The higher x_{tot}, the more bonds are formed and thus the higher the cross-link density. We can define the conversion at the gel point as x_{gel}, given by the Flory-Stockmayer theory:

$$x_{gel} = \frac{1}{\sqrt{R(f_F - 1)(f_M - 1)}} \tag{8}$$

$$= \frac{1}{\sqrt{1 \cdot (6-1)(2-1)}} \tag{9}$$

$$= 0.447 \tag{10}$$

where
x_{gel} is gel conversion
R is $\frac{n_{maleimide}}{n_{furan}}$
f_F is functionality of furan
f_M is functionality of maleimide.

At conversions below x_{gel}, there is no longer a network and the material will exhibit viscous flow.

The resulting material properties during an imposed time–temperature profile can be simulated based on these equations. To this end, the in-house developed software toolbox MATKIN was used.[34,35] This toolbox also calculates the molecular weight of the polymer, and from these values, the viscosity is obtained. As a power law describes the relationship between molecular weight M_W and viscosity η, experimental viscosity values obtained using rheometry are plotted against the simulated molecular weight.[36] The best fit for this power law was found as

$$\eta = 0.0191 \cdot M_W^{0.25}. \tag{11}$$

Methods

Dynamic mechanical analysis. The viscoelastic properties of the DA polymer DPBM-FT5000 were measured on a TA Instruments Q800 dynamic mechanical analyzer equipped with a film tension clamp, using an oscillatory strain of 0.1%, frequency of 1 Hz, and 125% force tracking. Heating was done at a temperature ramp of 10 K/min. The glass transition temperature (T_g) is considered the temperature point where the loss modulus is maximal.

On the same equipment, tensile testing was performed at room temperature with open furnace. The strain rate was set to $1\%s^{-1}$ until fracture with an initial static force of 0.001 N.

Rheometry. Dynamic rheometry is performed on a TA Instruments Discovery Hybrid Rheometer to determine T_{gel}. This temperature is defined as the temperature at which the phase shift δ, the loss angle, is independent of the oscillation frequency.[37] The analysis was done using aluminum parallel plates (diameter 14 mm) while accounting for thermal expansion.

The analysis was performed by first heating the samples to 120°C for 10 min, afterward the sample was cooled to 80°C and stepwise heated back to 120°C. Each step consists of increasing the temperature with 1°C and staying isothermal for 10 min before performing the measurement. The measurements were done by subjecting the sample to an oscillatory strain with an amplitude of 10% at different frequencies: 10, 6.31, 3.98, 2.51, 1.58, and 1 Hz.

Surface topography analysis. Two types of surface topography analysis were performed: white light interferometry and stylus profilometry. The white light measurements were done using a ContourGT-I 3D optical microscope with a reported repeatability of 0.02 nm and a step height accuracy ≤0.75%. The stylus (contact) measurements were made on a Veeco Dektak 8. The machine has a reported repeatability of 0.75 nm and an accuracy of 2%.

Material Properties

To get the process parameters of the filament extruder and the three dimensional (3D) printer right, the DA DPBM-FT5000 network is first characterized. Afterward, the processes of healing and extrusion are explained for this specific material.

Characterization

DPBM-FT5000 is first characterized using dynamic mechanical analysis (DMA), using the methods described in the Methods section. The DMA results (Fig. 3a) show a T_g of

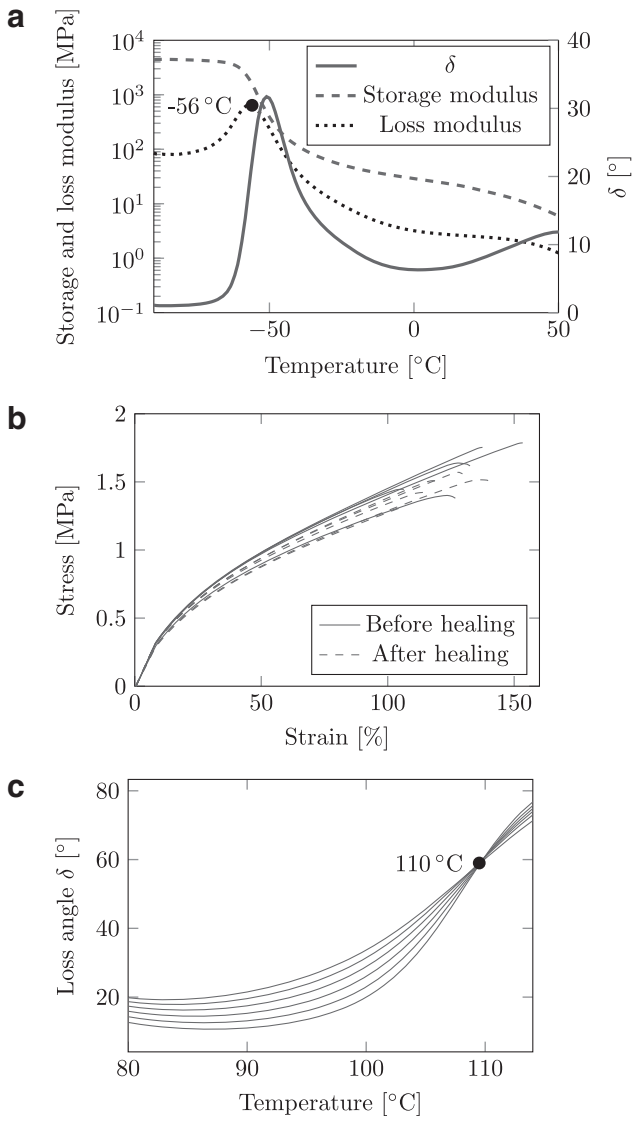

FIG. 3. **(a)** DMA results of DPBM-FT5000 show a T_g of −56°C. Measurement performed on a sample of size $9.85 \times 5.51 \times 0.80\,mm^3$. **(b)** Comparison of tensile tests before and after healing at 90°C for 30 min. **(c)** Rheometry measurements show a T_{gel} of 110°C. DMA, dynamic mechanical analysis.

−56°C, a storage modulus at room temperature (25°C) of 16.7 MPa, and a loss modulus of 2.43 MPa, and a low tan δ of 0.145, indicating elastic behavior. A stress–strain test (Fig. 3b) indicates that Young's modulus is 8.2 MPa with a fracture strain of 131% and fracture stress of 1.60 MPa. After healing for 30 min at 90°C and resting for 3 days at 30°C, these properties are 95% recovered. These measurements also show that the material is flexible enough at room temperature to be used for soft robotics.

Dynamic rheometry was performed to determine T_{gel}, as described in the Methods section. For every frequency, a line is plotted, the intersection of these lines shows the temperature at which the loss angle δ is frequency independent, which is T_{gel}.[37] T_{gel} is determined to be 110°C (Fig. 3c), indicating that processing should be done slightly above this temperature to have enough flow in the polymer.

Healing

To heal cracks or cuts, the DA material can be heated to 90°C, still $<T_{gel}$. This shifts the chemical equilibrium toward the reactants, breaking reversible bonds. Because of a decreased cross-link density, the mobility on a microscopic level is increased, allowing to slowly fill cracks. After 30 min at this temperature, the cracks are sealed, and the material can be slowly cooled down to room temperature, shifting the equilibrium back toward the DA adducts, restoring the network. Because at room temperatures the kinetics are relatively slow [Eq. (2)], it takes 24 h to reach the equilibrium cross-link density and hence full recovery of the initial mechanical properties. As heat is required to accelerate the healing, the polymer is classified as a nonautonomous self-healing system. This is not necessarily a drawback, as it allows for more control over the healing process.[16]

3D printing

To understand the behavior of the DA polymer during the extrusion and 3D-printing process, it is important to take a closer look at the chemical nature of the material. Moreover, this will explain the differences and developments needed compared with conventional thermoplastic materials (e.g., polylactic acid [PLA], NinjaFlex).

Conventional 3D-printing materials lose their structural stability at higher temperature because their crystalline phase is melted, in case of semicrystalline polymers such as PLA (at 230°C), or because they are heated well above their glass transition, as for amorphous acrylonitrile butadiene styrene (ABS) (at 195°C). Above these melting/glass transition temperatures, the polymer exhibits a viscous flow behavior, which makes filament extrusion and 3D printing possible.

As these self-healing DA materials do not show a melting range and are still a network when heated above their glass transition, this principle cannot be used. The principle behind its extrusion process is fundamentally based on the thermoreversible DA reaction, making it a form of reactive printing. Reactive extrusion of DA material follows a temperature profile as illustrated in Figure 4. It is first heated $>T_{gel}$ to break enough DA bonds to have a viscous flow behavior. As it is heated further, its viscosity further decreases. In this liquid state, the material can be extruded through the nozzle.

After extrusion, the material needs to solidify quickly for structural rigidity of the part. As the solidification involves the re-establishing of the network through the DA reaction, the temperature should be kept as high as possible, to accelerate the reaction kinetics [Eq. (2)], but still $<T_{gel}$ to allow network formation (Fig. 4). Once the network has formed, the material can be cooled to ambient temperature. After 24 h at room temperature, the initial properties are recovered.

Results

Filament extrusion

Before the 3D-printing process, the filament itself had to be produced. The filament was extruded on a 3DEVO NEXT extruder, consisting of four heating zones whose temperatures can be set independently, two adjustable fans, an interchangeable die, a diameter feedback system, and a motor with adjustable speed. To prepare the polymer pellets typically used in extrusion processes, a solvent-cast sheet of DPBM-FT5000

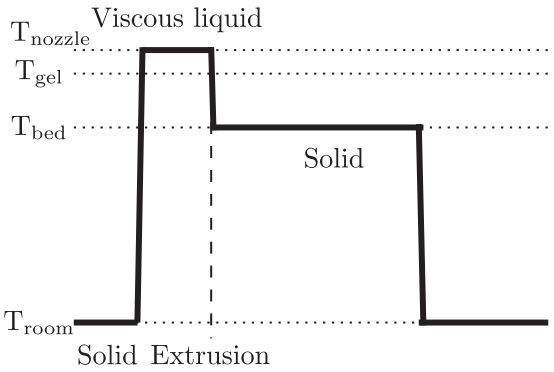

FIG. 4. The thermoreversibility of the DA material is exploited for extrusion. Therefore, an adapted heating scheme is needed in comparison with conventional 3D-printed materials. 3D, three-dimensional.

was cut into cubes of $\sim 2 \times 2 \times 2$ mm, which were fed in the extruder. The main parameters to be determined are the four heater temperatures and the screw speed of the motor.

Experimental

Starting from the material properties, the fine-tuning of the extruder settings was optimized experimentally. However, during this optimization, the thermal behavior of the material is not the only aspect that needs to be considered.

When increasing the screw speed, a sharkskin pattern appeared on the extruded filament (Fig. 5a), caused by a flow instability resulting from a higher buildup of viscoelastic stresses.[38] To prevent this, the extruder screw speed was reduced. As this setting is limited by the extruder software to 2 rpm, this speed was used.

If the temperature is set too low, the material remains too elastic for extrusion and a shear failure phenomenon is observed in the filament (Fig. 5b). This is induced by the rotation of the screw. Owing to the viscoelastic behavior of the polymer, the internal stresses that did not relax (sufficiently) in the die can relax after exiting the die, making the filament curl. These internal stresses can be relaxed by increasing the time spent in the die. To achieve this, the extruder screw speed can be reduced, but to prevent the sharkskin effect, this was already set to the lowest possible.

Another solution is to make the die longer and have a more gradual diameter reduction, such that the material is able to relax in the die. The die that was delivered with the extruder has an inner diameter of 4 mm, which is more than the desired filament diameter of 2.85 mm; however, the extruder design leads the filament through a diameter-reducing system before spooling. Owing to the slow solidification kinetics of the DA material, leading the filament through the diameter reduction system flattens the filament too much. Therefore, the diameter reduction system of the NEXT extruder was not used. To overcome this, a custom die was made with a smaller diameter (2 mm), taking into account the die swell ratio of the material. The final design is shown in Figure 5d.

After optimizing the extrusion process, visually smooth and consistent filament (Fig. 5c) can be extruded continuously, which can be used for the 3D-printing process. The following parameters were eventually used:

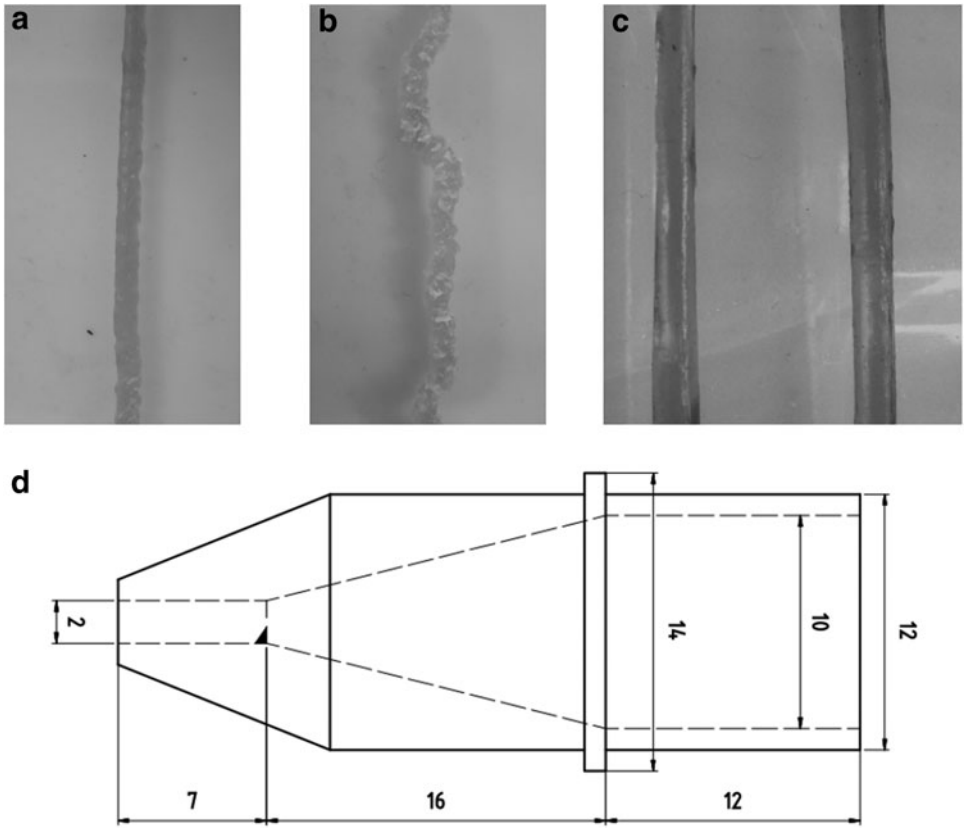

FIG. 5. Schematics of the die and close up of filaments strands prepared using the adapted extruder. **(a)** High shear stresses and stress relaxation make the filament curl at too low temperatures. **(b)** Sharkskin effect as a process instability due to high flow rates. **(c)** The resulting filament is quite smooth and has a consistent diameter. **(d)** Detailed drawing of the adapted nozzle.

screw velocity: 2 rpm,
heater 4: 80°C (measured 88°C),
heater 3: 100°C (measured 106°C),
heater 2: 108°C (measured 113°C), and
heater 1: 103°C (measured 109°C).

Note that these are lower than the simulated values in the Filament Extrusion section, which is due to an offset in the machine's thermocouple measurements. The measured values are taken at the outside of the heater zones, and are closer to the real temperatures inside the machine. The roughness of the filament was measured using white light interferometry, as shown in Figure 8a, giving an area roughness value (S_a) of 2.177 μm.

Simulation

The chemical reactions and the resulting property changes during the extrusion process were simulated to verify the flow behavior and to be able to predict the settings for other DA polymers in the future.

If the extrusion temperatures are set slightly lower than T_{gel}, the material is prevented from degelling, but the mechanical breaking of bonds in the very soft network might allow enough flow of the material to allow successful extrusion. Setting the temperature too high lowers the viscosity too much and the material will drip through the die. Using this knowledge, the temperature profile was determined by trial and error such that the material degels during the process and gels again before coming out of the nozzle.

For the DPBM-FT5000 material passing through the 3DEVO NEXT extruder, the temperature profile was calculated for a screw rotation speed of 2 rpm (Fig. 6a). The evolution of total conversion resulting from this temperature profile was simulated using the MATKIN simulation software described in the Reaction Kinetics section.

The simulation of the extrusion process, as shown in Figure 6a, indicates that there is a 300 s zone around the 600 s mark where the total conversion x_{tot} dips below the critical (de-)gel conversion $x_{gel} = 0.447$ (indicated with a horizontal line). After this zone where the material can flow, it gels again, right before coming out of the nozzle. This simulation also learns that after extrusion, the process of reaching equilibrium conversion could be sped up by heating the filament slightly.

With this information, the extruder settings can in the future be predicted for other self-healing DA materials having different mechanical properties. Using this technique, multimaterial actuators[20] can in the future also be 3D printed instead of molded.

3D printing

Simulation. At first, the evolution of total DA conversion during printing was simulated using the in-house developed software MATKIN (the Reaction Kinetics section). Unlike for the filament extrusion process, most FFF printers have only two controllable temperatures (in addition to other settings such as extrusion velocity): the temperatures of the heater block and of their heated bed or environment. The temperature profile the material undergoes during printing depends on the 3D printer and the settings chosen. The filament is at room temperature when it enters the heater block of the 3D printer and is heated up to the print temperature. Next, it is deposited on the heated bed (Fig. 4). The time t_h spent in the heater block is in good approximation determined by

$$v_f = \frac{d_n^2 v_n}{d_f^2} \text{ (conservation of mass)} \tag{12}$$

$$t_h = \frac{l_h}{v_f} \text{ (filament velocity)} \tag{13}$$

so that

$$v_n = \frac{l_h \cdot d_f^2}{d_n^2 \cdot t_h}, \tag{14}$$

where
d_n is nozzle diameter (mm),
d_f is filament diameter (mm),
v_n is print velocity (mm/s),
v_f is filament velocity (mm/s), and
l_h is heater block length (mm).

This gives a relation between the time spent in the heater block, which is important as the material needs to degel before printing, and the printing velocity v_n.

d_n, d_f, and l_h are constrained by the choice of 3D printer, which is in this case an open-source LulzBot TAZ 6 ($d_n = 0.4$ mm, $d_f = 2.85$ mm, $l_h = 25$ mm). The maximal print velocity depends on the temperature-dependent reaction kinetics as the polymer has to degel as close as possible to the moment it exits the nozzle, meaning that t_h has to be high enough for the polymer to degel. This also indicates that the print temperature and maximal velocity will always be coupled. As there is only a limited temperature range in which the material has a viscosity suitable to be printed, this printing velocity is imposed rather than a free parameter.

A sidenote has to be made here: during the print process, there is also ''travel'' time during which the extruder is moving but is not extruding filament, this time is not considered during the simulations, as it is highly irregular and depends on the 3D-model being printed. This will be overcome during the experimental part by setting the travel speed high, reducing this time to the minimum, while shortening the print time. Each layer needs to solidify before the next layer is deposited on top of it to avoid deformation during the printing of the next layer. Hence, a fast solidification of the printed material is an important factor, determining the print time and the achievable resolution.

By simulating the isothermal behavior of the DA material at different temperatures, the evolution of viscosity (Fig. 6b) and total conversion (Fig. 6c) during the printing process were estimated. At higher temperatures, the material degels faster, but the total conversion and viscosity will eventually also be lower. As the material degels faster (total conversion becomes lower than x_{gel}), t_h can be lower, resulting in the possibility to print faster. At 115°C, the material takes 740 s to degel, which equals a maximal printing velocity of 2 mm/s.

Although increasing the temperature from 115°C to 130°C allows to increase print velocity to 41 mm/s [Eq. (14)], these velocities are below those that can be achieved while printing other soft polymers.[39,40] In theory, all temperatures $>T_{gel}$ can be used to print, but the closer to T_{gel}, the slower the material can be printed. Printing at higher temperatures is to be avoided as irreversible side reactions can take place >120°C.

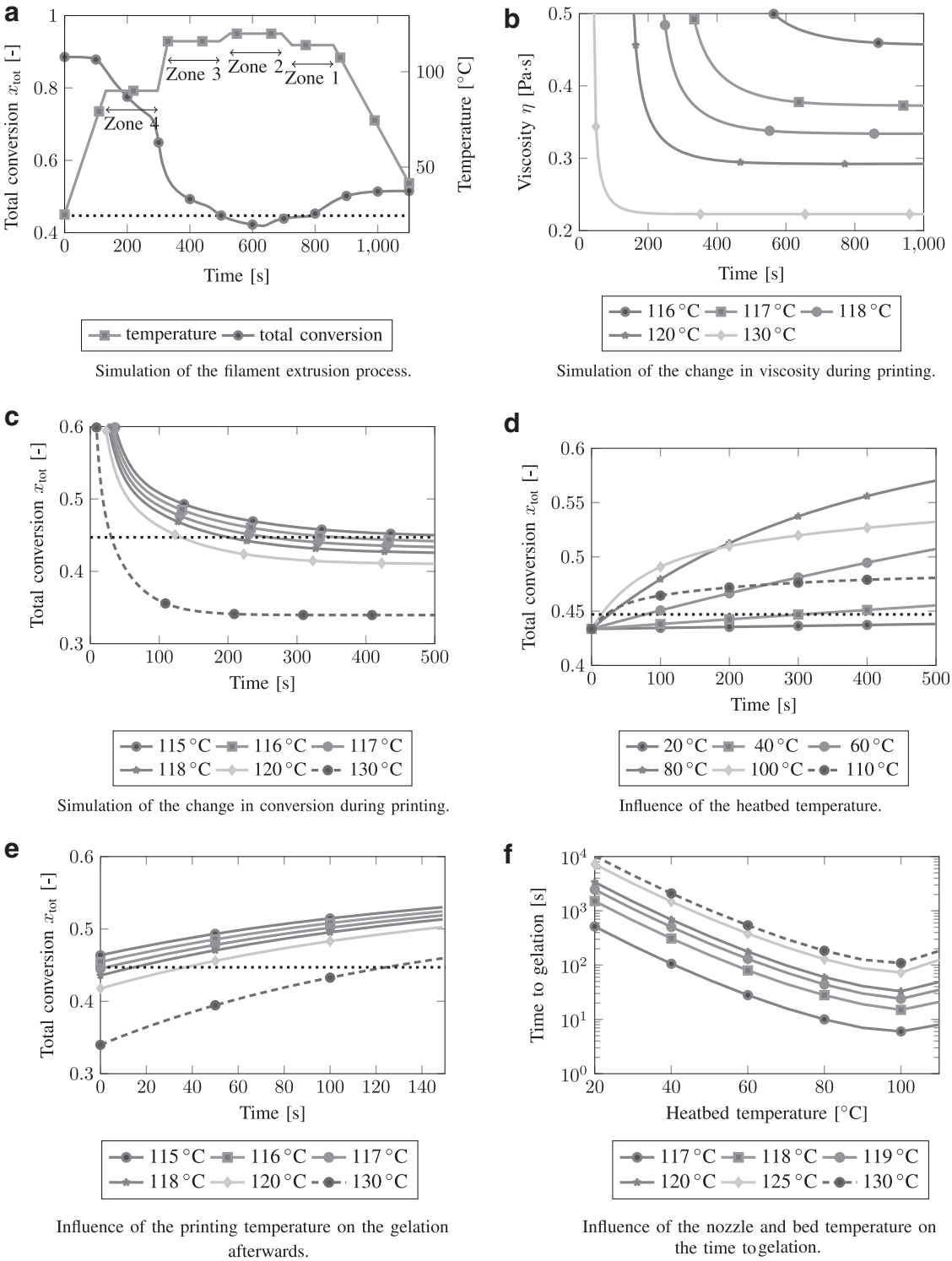

Simulation of the filament extrusion process.

Simulation of the change in viscosity during printing.

Simulation of the change in conversion during printing.

Influence of the heatbed temperature.

Influence of the printing temperature on the gelation afterwards.

Influence of the nozzle and bed temperature on the time to gelation.

FIG. 6. **(a)** Simulations (steps of 1 s) of the extrusion process show that the material only degels (total conversion below the (de-)gelation line of $x_{gel} = 0.447$) for ~ 300 s. Screw rotation speed is set at 2 rpm. **(b)** Simulations of the change in viscosity during printing at various temperatures show that at a lower print temperature, the kinetics of degelation are slower and the material will remain more viscous. **(c)** At higher temperatures, degelation can take place faster. **(d)** The heated bed temperature has a large influence on the time it takes for the printed material to gel. This time should be minimal to allow faster printing and prevent flow of the printed material. Consequently a higher temperature is beneficial, with an optimum at 100°C. **(e)** A higher printing temperature has a negative effect on the time to gelation on the heatbed. **(f)** The time to gelation depends on the print temperature and the heatbed temperature (lines). Gelation happens earlier at low print temperatures and high heatbed temperatures.

Also the influence of the heatbed temperature on the gelation of the reversible network is simulated (Fig. 6d). If a heated bed is considered, these simulations are only valid for the first few layers, whereas if a heated environment is considered, they are valid for the whole part. The graphs are presented such that the origin of the time axis is placed at the moment of extrusion, after the filament has been heated in the heater block of the 3D printer for $t_h = 260$ s, which corresponds to approximately $v_n = 5$ mm/s.

The simulation in Figure 6d clearly shows that a higher environmental temperature allows for faster reaction kinetics, faster gelling (conversion $x_{tot} > x_{gel} = 0.447$, indicated as a dotted line), and formation of the network, and thus, the faster a new layer can be deposited on top. However, also here an optimum is observed. Setting the heatbed to 110°C results in a slower gelation than at 100°C, because the driving force for the reaction, the difference between the equilibrium conversion and the actual conversion, is low. At 100°C, there is an optimum between this driving force and the kinetics of the reaction. Above T_{gel}, gelation will not happen.

The time to gelation does not only depend on this environmental temperature, but also depends on the print temperature (at the nozzle), as shown in Figure 6e. This also indicates that there is a compromise to be made: printing velocity versus time to gelation afterward. The combined impact of the heatbed temperature and printing temperature on the time to gelation is shown in Figure 6f. In general, these kinetic simulations show that the ideal situation is to print at a temperature–velocity combination for which the network just degels in the nozzle, preferably with the temperature only slightly $>T_{gel}$ and to have the heated bed set just $<T_{gel}$ to speed up the gelation kinetics. However, with the print temperature just $>T_{gel}$, the printer should print at low speeds. Therefore, the optimal settings are determined to be a nozzle temperature of 117°C and heatbed temperature of 100°C.

Experimental. The conclusion of the simulations gives a good idea of the printer settings, but there are practical considerations that have to be taken into account.

The same object (a 20 × 20 mm sheet) was printed with the filament at room temperature, with the heated bed at 90°C due to limitations on the advised operating conditions of the electronics, but using various extrusion temperatures (Fig. 7). It was found that indeed at low temperatures (115–117°C), more detail is left in the print and the dimensional accuracy is higher, whereas at higher temperatures, the material flows too much after deposition and the details are lost. At temperatures <115°C, the material was unable to flow consistently out of the nozzle and no satisfactory samples were obtained. At ≥120°C, the print quality drops, bubbles are visible and the flow becomes inconsistent (Fig. 7c). Moreover, irreversible bonds may start to form at these temperatures. The optimal settings are determined as:

print temperature 117°C,
heated bed temperature 90°C, and
print velocity 5 mm/s.

The heated bed temperature is chosen as 90°C because of practical limitations of the printer. A printing temperature of 117°C is preferred because the result is smoother and the printing speed can be increased to 5 mm/s.

Print quality. Dimensional accuracy was evaluated by comparing the dimensions of the digital 3D model and the printed part. Seven 20 × 20 mm samples were printed under the same conditions ($v_n = 5$ mm/s, heated bed temperature 90°C, print temperature 117°C). Measuring them in both directions using a caliper gives a mean error of 0.28 mm (1.4%) with a standard deviation of 0.18 mm.

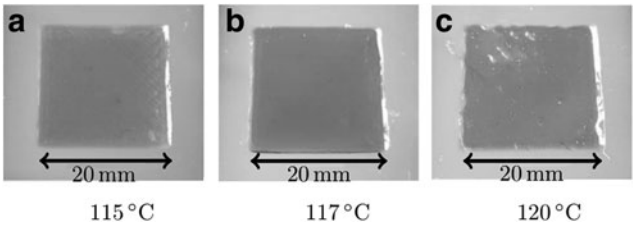

FIG. 7. A set of test specimens of 20 × 20 mm sheets printed at different extruder temperatures, but the same bed temperature of 90°C and printing speed 5 mm/s. At 115°C, the line marks are still slightly visible, whereas these are gone at 117°C. At 120°C, the quality deteriorates. At 115°C **(a)**, the line marks are still slightly visible, whereas these are gone at 117°C **(b)**. At 120°C **(c)**, the quality deteriorates.

As the fastest gelation times for DPBM-FT5000 are ~7 s (Fig. 6f, taking into account the optimal settings and practical limitations), printing overhangs or ''bridging'' spans between pillars or wall sections are not feasible with this material. A reduction of the gelation time to ≤1 s would be required. Instead, overhang should always be printed with support material.

Owing to the low viscosity and the self-healing character, the typical layer and line marks of the 3D-printing process (FFF) are not visible after printing, as is clearly shown in Figure 7b. Owing to the continued elevated temperature after deposition, due to both the heated bed and the deposition of layers on top,[41] the successive layers become covalently bonded to each other without the need of post-treatments. This allows to print airtight components, an important feature in soft pneumatic robotic systems. Moreover, this absence means that the surface does not have ridges where dirt, bacteria, or fungi can settle, which is an important property in a potential application field of this technology: soft grippers for pick and placing delicate items in the food industry.

Another structural advantage of this technique is that the printed parts have an improved isotropy in mechanical properties. Anisotropy resulting from the layer-by-layer process is generally a problem for parts made by FFF, as the adhesion between different layers is reduced due to the voids occurring by depositing cylindrical paths next to each other.[42] The interlayer connections rely on relatively weak

Table 1. Comparison of the Measured Mechanical Properties in Different Print Orientations

Print angle	*Fracture stress (MPa)*	*Fracture strain (%)*	*Young's modulus (MPa)*
0° ($n = 5$)	2.02 ± 0.17	100 ± 18	8.22 ± 0.97
45° ($n = 4$)	2.19 ± 0.14	90.1 ± 4.6	8.11 ± 0.83
90° ($n = 4$)	2.29 ± 0.21	91.8 ± 8.8	8.5 ± 1.5
p	0.88	0.105	0.483

A one-way ANOVA is performed for each mechanical property, the resulting p-values are added to this table. Data are obtained from a controlled strain rate tensile test as described in the Methods section.

TABLE 2. COMPARISON OF THE MEASURED ANISOTROPY OF SEVERAL (COMMERCIAL) FLEXIBLE MATERIALS IN THE 45° AND 90° DIRECTIONS COMPARED WITH THE 0° DIRECTION

	Fracture stress		*Fracture strain*		*Young's modulus*	
Material	*Anisotropy 45° (%)*	*Anisotropy 90° (%)*	*Anisotropy 45° (%)*	*Anisotropy 90° (%)*	*Anisotropy 45° (%)*	*Anisotropy 90° (%)*
DPBM-FT5000	−8.4	−13.4	9.9	8.2	1.3	−3.2
NinjaFlex	55.0	65.8	25.0	32.4	14.3	28.6
SemiFlex	50.7	74.3	28.3	43.4	15.0	27.5
Cheetah	70.0	81.3	38.2	58.2	16.7	31.0
T-Lyne	98.0	99.2	96.7	97.8	16.7	27.8

DPBM-FT5000 has significantly lower values than the commercial materials. Adapted from Yang *et al.*[32]

noncovalent interactions and limited physical bonding at the layer interface (driven by interlayer chain entanglements), as a result the mechanical strength is very often limited in the direction perpendicular to the print direction.

This also implies that the print direction is important for the mechanical properties of the part. To test the isotropy in 3D-printed self-healing parts, a thin sheet was printed unidirectionally ($v_n = 5$ mm/s, heated bed temperature 90°C, print temperature 117°C). Samples were punched in the 90°, 45°, and 0° directions. Table 1 shows that there are only small variations in mechanical properties at the different angles. To determine whether these differences are statistically relevant, a one-way analysis of variance is performed. Based on the *p*-values (Table 1), it is impossible to reject the null hypothesis, namely that all samples come from the same normal distribution.

If we define anisotropy as (equivalently for ε_{ult} and E)

$$\text{Anisotropy} = 100 \cdot \frac{\sigma_{\text{ult, }0^\circ} - \sigma_{\text{ult, }90^\circ \text{ or } 45^\circ}}{\sigma_{\text{ult},0^\circ}}, \qquad (15)$$

it can be said that most probably there is no anisotropy present after 3D printing of the DPBM-FT5000

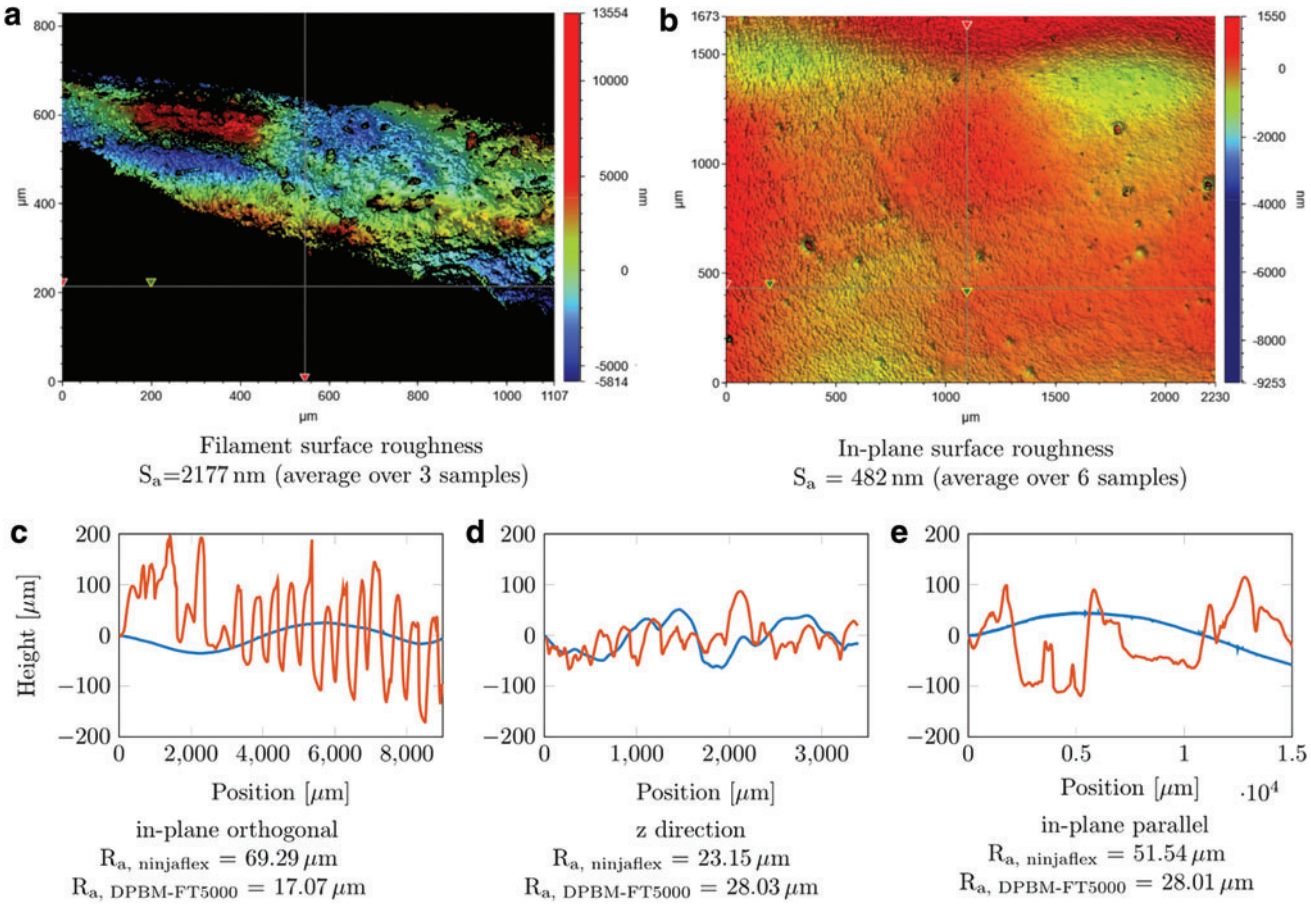

FIG. 8. **(a, b)** Surface roughness measured by white light interferometry, no value was obtained in the *black* areas of **(a)** due to the cylindrical shape of the filament. **(c–e)** Roughness profiles in different directions of unidirectional printed samples DPBM-FT5000 (*blue*) and NinjaFlex (*red*). Both samples printed on a LulzBot TAZ 6 with a layer height of 0.3 mm and nozzle size 0.5 mm. NinjaFlex printed at 230°C. Profiles measured with a stylus radius of 2.5 μm and force of 3 mg, tilt of the sample is accounted for. Color images are available online.

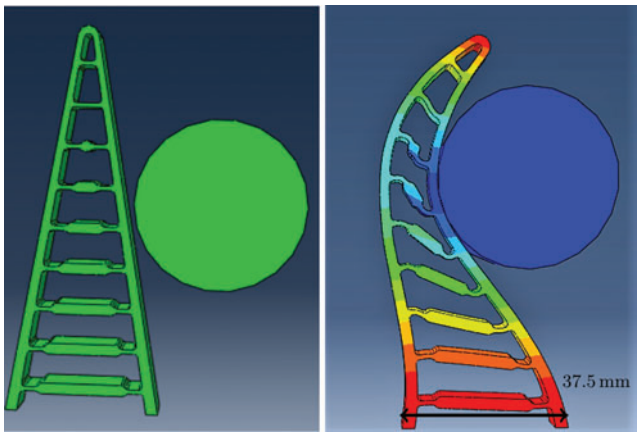

FIG. 9. Finite element analysis (Abaqus CAE) illustrates the grasping concept. The finger will move toward and around the object (a 40 mm cylinder), and thus grasp it. Color images are available online.

thermoreversible network. In Table 2, the anisotropy values for different (commercial) flexible materials are tabulated, as are the values for the self-healing polymer. This indicates that there is indeed a problem regarding anisotropy in FFF (with anisotropy values up to 99%!). From the table it can be concluded that the printed DA network has anisotropic values that are an order of magnitude lower than those of the conventional flexible printable polymers. Owing to the low viscosity of the degelled DA polymer, no voids are created at the interface. In addition, after printing, a high concentration of DA covalent bonds is formed across the layer interface. The very low anisotropy value of Young's modulus indicates that the strain response to an applied stress is almost isotropic.

Using a stylus profilometer, the surface roughness of the printed DA part was measured (Fig. 8), and compared with a NinjaFlex sample. In the in-plane direction orthogonal to the printed lines, it becomes clear that the self-healing material has a smoother surface than the NinjaFlex sample. In general, the fluctuations in the DPBM-FT5000 part are also of a lower

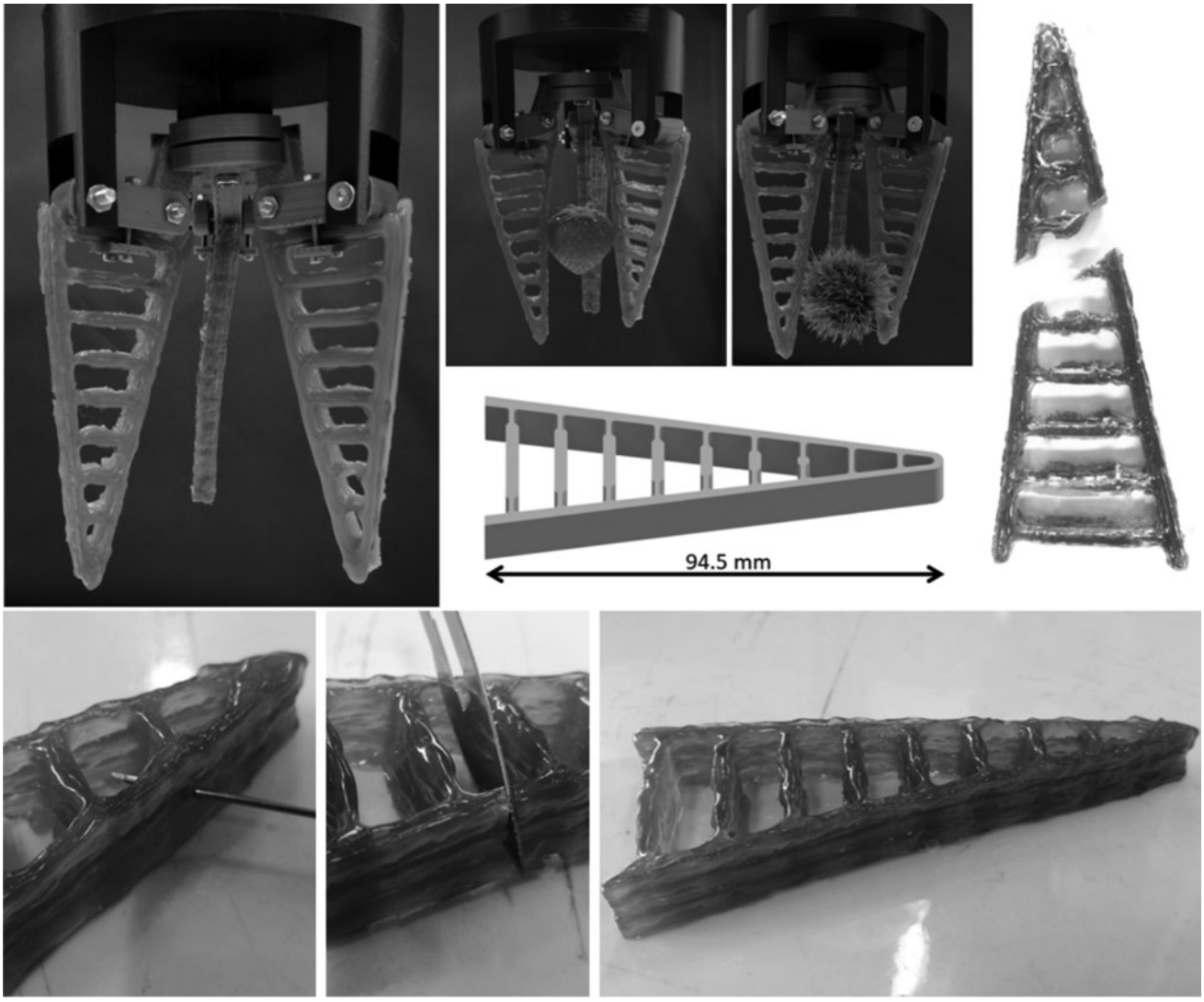

FIG. 10. Three 3D-printed self-healing DHAS fingers are placed in a circular pattern to form a gripper. The gripper is able to handle various objects, both soft and hard. The fingers were subjected to different damaging conditions, both nonfatal (puncture, cut) and fatal (sliced in half) and are able to recover from it with only small visual scars (*lower right*).

frequency. In the z-direction, both materials show a comparable roughness amplitude, indicating that no significant improvement is made in this direction. Parallel to the in-plane print direction, there is a slightly smaller amplitude, but again a much lower frequency is observed than NinjaFlex. Figure 8b shows the in-plane surface analyzed by white light interferometry, the S_a value of 482 nm is $\sim$4.5 times lower than the filament it was printed with. This lower roughness can be of great importance in the food industry since it decreases the potential of dirt and bacteria to get stuck in the ridges on the surface. Less extensive washing and other decontamination methods need to be used, which saves time and often reduces the consumption of water and cleaning products.

A 3D-Printed Self-Healing Soft Actuator

To demonstrate the use of the developed FFF technique, a soft gripper is manufactured. The chosen design is the adaptive gripper DHAS with FinRay effect designed by the FESTO Automation Company.[43] Each finger is A shaped with several cross-beams. Its symmetry makes it a very versatile gripper, as it is able to grasp objects from both sides. The original FESTO grippers are made of thermoplastic polyurethane. As the material that is used in this study is different, a finite elements analysis using ABAQUS was performed on the model of a single finger to validate the ability to grasp objects (Fig. 9). A cylinder with diameter 40 mm is used for this demonstration, as convex objects are easier to grasp because of increased contact with the object.

The design consists of thin connected beams, making it impossible or at least very difficult to manufacture using previously developed techniques for the DA polymer (molding, shaping-through-folding-and-self-healing). The de-molding step would be crucial, potentially damaging the part. Although it would be possible to manufacture these grippers by shaping-through-folding-and-self-healing, cutting all these beams and healing them together would be labor intensive; moreover, this technique would leave a high variation between different fingers. This shows that 3D printing not only increases the design freedom of these self-healing soft actuators, but also gives a more reproducible result.

Three of these fingers were 3D printed in the self-healing DPBM-FT5000 material. They are 10 mm thick, and measure 94.5 mm from top to bottom. The fingers are placed in a circular pattern and connected to a base with an actuation system that was 3D printed in PLA using the same LulzBot TAZ 6 (Fig. 10). Each finger is mounted on a tilting plate and held in place by a smaller plate. The three tilting plates are connected to a center that can move vertically. In the center, a locknut is placed that holds a threaded rod. This rod is also connected to the base, such that turning the rod moves the center, and tilts the fingers, which creates the grasping motion.

The printed three-fingered gripper is demonstrated. It is able to grasp different objects. To illustrate the ability to heal, the fingers are damaged in different ways, ranging from a small scratch to slicing them in two (see Fig. 10). The fingers are healed by placing them in an oven at 90°C for 30 min. Afterward, they are left to recover at room temperature for 24 h. Small scratches can also be repaired by locally heating them with a soldering iron on the lowest temperature setting. Under all of these damaging conditions, the fingers were able to heal. Owing to small misalignments during the healing process, some scars can remain visible.

Conclusion

Self-healing soft robots have shown great potential for adoption in industry. The fabrication methods first developed were limited to shaping-through-folding-and-self-healing and molding. As both methods have their limitations regarding design flexibility, a novel additive manufacturing procedure (FFF) for self-healing DA materials was developed in this study. For the self-healing material studied in this work, the flowing and solidification process is based on the kinetics of the thermoreversible DA reaction, rather than on melting and crystallization, used in FFF of conventional flexible polymers. The process consists of two major steps: extrusion of the filament and the 3D printing itself. In this research, for a DPBM-FT5000 DA polymer, the process parameters for filament extrusion were derived through modeling of the DA reactions during the shaping process and through experimental fine tuning. With some customizations of an extruder platform, the self-healing elastomer could be successfully extruded into a 2.85 mm diameter filament, which can be used by FFF 3D printers. The obtained DPBM-FT5000 filament was used in a direct extruder FFF 3D printer and Lulzbot TAZ 6 printer. The process parameters of the actual printing were again derived using both simulations and experimental fine-tuning. The parts produced proved to be more smooth than commercial soft polymers, which is an advantage in, for example, the food industry (avoids bacteria growth in the seams). Moreover, an important structural advantage is the isotropy in mechanical properties after printing. The developed additive manufacturing technique is demonstrated by the filament printing of a soft gripper based on the DHAS actuators developed by FESTO. The functionality of this gripper was validated by gripping different objects while the healing ability is illustrated by completely recovering from large macroscopic cuts. The FFF approach developed in this study allows future self-healing soft robots to be manufactured with more design freedom and less manual effort.

Acknowledgments

The authors thank Prof. Heidi Ottevaere and her team (BPHOT, VUB) for performing the surface roughness measurements.

Author Disclosure Statement

No competing financial interests exist.

Funding Information

This research is funded by the FWO (Fonds Wetenschappelijk Onderzoek): SBO project AMSeR (G028218N) and personal FWO-grants of Roels (1S84120N), Terryn (FWOTM784) and Brancart (12W4719N), and by the EU FET Project SHERO (828818).

References

1. Trivedi D, Rahn CD, Kier WM, *et al.* Soft robotics: biological inspiration, state of the art, and future research. Appl Bionics Biomech 2008:5;99–117.
2. Manti M, Hassan T, Passetti G, *et al.* A bioinspired soft robotic gripper for adaptable and effective grasping. en. Soft Robot 2015:2;107–116.
3. Marchese AD, Katzschmann RK, Rus D. A recipe for soft fluidic elastomer robots. Soft Robot 2015:2;7–25.

4. Day N, Penaloza J, Santos VJ, *et al.* Scalable fabric tactile sensor arrays for soft bodies. J Micromech Microeng 2018: 28;064004.
5. Martinez RV, Fish CR, Chen X, *et al.* Elastomeric origami: programmable paper-elastomer composites as pneumatic actuators. Adv Funct Mater 2012:22;1376–1384.
6. Tolley MT, Shepherd RF, Mosadegh B, *et al.* A resilient, untethered soft robot. Soft Robot 2014:1;213–223.
7. Rus D, Tolley MT. Design, fabrication and control of soft robots. Nature 2015:521;467–475.
8. Gorissen B, Reynaerts D, Konishi S, *et al.* Elastic inflatable actuators for soft robotic applications. Adv Mater 2017:29; 1604977.
9. Giannaccini ME, Georgilas I, Horsfield I, *et al.* A variable compliance, soft gripper. Auton Robots 2014:36;93–107.
10. Amend J, Cheng N, Fakhouri S, *et al.* Soft robotics commercialization: jamming grippers from research to product. Soft Robot 2016:3;213–222.
11. Terryn S, Mathijssen G, Brancart J, *et al.* Toward self-healing actuators: a preliminary concept. IEEE Trans Robot 2016:32;736–743.
12. Cao J, Lu C, Zhuang J, *et al.* Multiple hydrogen bonding enables the self-healing of sensors for human–machine interactions. Angew Chem Int Ed 2017:56;8795–8800.
13. Cordier P, Tournilhac F, Soulíe-Ziakovic C, *et al.* Self-healing and thermoreversible rubber from supramolecular assembly. Nature 2008:451;977–980.
14. Cromwell OR, Chung J, Guan Z. Malleable and self-healing covalent polymer networks through tunable dynamic boronic ester bonds. J Am Chem Soc 2015:137; 6492–6495.
15. Cuvellier A, Verhelle R, Brancart J, *et al.* The influence of stereochemistry on the reactivity of the Diels–Alder cycloaddition and the implications for reversible network polymerization. Polymer Chem 2019:10;473–485.
16. Terryn S, Brancart J, Lefeber D, *et al.* Self-healing soft pneumatic robots. Sci Robot 2017:2;eaan4268.
17. Terryn S, Brancart J, Lefeber D, *et al.* A pneumatic artificial muscle manufactured out of self-healing polymers that can repair macroscopic damages. IEEE Robot Autom Lett 2018:3;16–21.
18. Scheltjens G, Diaz MM, Brancart J, *et al.* A self-healing polymer network based on reversible covalent bonding. React Funct Polym 2013:73;413–420.
19. Diaz MM, Brancart J, Van Assche G, *et al.* Room-temperature versus heating-mediated healing of a Diels-Alder crosslinked polymer network. Polymer 2018:153;453–463.
20. Roels E, Terryn S, Brancart J, *et al.* A multi-material self-healing soft gripper. In: 2019 2nd IEEE International Conference on Soft Robotics (RoboSoft). Seoul, South Korea: IEEE, 2019, pp. 316–321.
21. Terryn S, Mathijssen G, Brancart J, *et al.* Development of a self-healing soft pneumatic actuator: a first concept. Bioinspiration Biomimetics 2015:10;046007.
22. Gorissen B, Hoof CV, Reynaerts D, *et al.* SU8 etch mask for patterning PDMS and its application to flexible fluidic microactuators. Microsyst Nanoeng 2016:2;16045.
23. Udupa G, Sreedharan P, Dinesh PS, *et al.* Asymmetric bellow flexible pneumatic actuator for miniature robotic soft gripper. 2014. Available at: https://www.hindawi.com/journals/jr/2014/902625/abs/ (accessed February 27, 2020).
24. She Y, Li C, Cleary J, *et al.* Design and fabrication of a soft robotic hand with embedded actuators and sensors. J Mech Robot 2015:7;021007.
25. Roppenecker DB, Pfaff A, Coy JA, *et al.* Multi arm snake-like robot kinematics. In: 2013 IEEE/RSJ International Conference on Intelligent Robots and Systems. Tokyo: IEEE, 2013, pp. 5040–5045.
26. Peele BN, Wallin TJ, Zhao H, *et al.* 3D printing antagonistic systems of artificial muscle using projection stereolithography. Bioinspiration Biomimetics 2015:10;055003.
27. Truby RL, Lewis JA. Printing soft matter in three dimensions. Nature 2016:540;371–378.
28. Robinson SS, O'Brien KW, Zhao H, *et al.* Integrated soft sensors and elastomeric actuators for tactile machines with kinesthetic sense. Extreme Mech Lett 2015:5;47–53.
29. Yap HK, Ng HY, Yeow C-H. High-force soft printable pneumatics for soft robotic applications. Soft Robot 2016:3;144–158.
30. Mutlu R, Alici G, Marc in het Panhuis, *et al.* 3D printed flexure hinges for soft monolithic prosthetic fingers. en. Soft Robot 2016:3;120–133.
31. Wallin TJ, Pikul J, Shepherd RF. 3D printing of soft robotic systems. Nat Rev Mater 2018:3;84–100.
32. Yang K, Grant JC, Lamey P, *et al.* Diels-Alder reversible thermoset 3D printing: isotropic thermoset polymers via fused filament fabrication. Adv Funct Mater 2017:27;1700318.
33. Yu K, Xin A, Du H, *et al.* Additive manufacturing of self-healing elastomers. NPG Asia Mater 2019:11.
34. Verhelle R, Assche GV. MATKIN: software to model kinetics and rheokinetics. 2019. Available at: https://www.vub.be/MACH/FYSC/equipment/MATKIN (accessed February 27, 2020).
35. Brancart J, Verhelle R, Mangialetto J, *et al.* Coupling the microscopic healing behaviour of coatings to the thermoreversible Diels-Alder network formation. Coatings 2019:9;13.
36. Fox TG, Flory PJ. Viscosity—molecular weight and viscosity—temperature relationships for polystyrene and polyisobutylene 1,2. J Am Chem Soc 1948:70;2384–2395.
37. Winter HH. Can the gel point of a cross-linking polymer be detected by the G0–G00 crossover? Polymer Eng Sci 1987: 27;1698–1702.
38. Guiu F, Pratt PL. Stress relaxation and the plastic deformation of solids. Phys Status Solidi B 1964:6;111–120.
39. Tek N. Printing guidelines. Available at: https://ninjatek.com/printing-guidelines/ (accessed February 1, 2019).
40. Recreus. Filaflex original 82A technical sheet. Available at: https://recreus.com/img/pdf/FILAFLEX%2082A%20TECHNICAL%20SHEET% 20&%20MSDS%202017.pdf (accessed February 1, 2019).
41. Vaes D, Coppens M, Goderis B, *et al.* Assessment of crystallinity development during fused filament fabrication through fast scanning chip calorimetry. Appl Sci 2019:9;2676.
42. Song Y, Li Y, Song W, *et al.* Measurements of the mechanical response of unidirectional 3D-printed PLA. Mater Design 2017:123;154–164.
43. FESTO. Adaptive gripper fingers DHAS. Available at: https://www. festo. com/cat/en - gb gb/data/doc ENUS/PDF/US/DHAS ENUS.PDF (accessed February 1, 2019).

Address correspondence to:
Bram Vanderborght
Robotics and Multibody Mechanics (R&MM)
Vrije Universiteit Brussel
Pleinlaan 2
1050 Elsene
Belgium

E-mail: bram.vanderborght@vub.be